Computational analysis of mitochondrial morphology and membrane potential

Alexandre Carnet
alexandre.carnet@tecnico.ulisboa.pt

Instituto Superior Técnico, Lisboa, Portugal

December 2015

Abstract

Mitochondria, organelles initially thought as static, have been receiving large focus allowing for their linkage to many different cellular mechanisms. Two important and frequently studied parameters, mitochondrial morphology and potential, provide significant insight into a cell's health state. In current literature, these features are often observed sequentially, and the correlation between them is consistently causal – after inflicting some external stimulus on the cell that affects either morphology or potential, a change on the other is observed. Predominantly, depleting mitochondrial potential eventually leads to the fragmentation of mitochondria, respiratory dysfunction and finally cell death. Nevertheless, the correlation between a mitochondrion's potential and morphology, independent of external factors, has been overlooked. Therefore, we set out to determine if such a correlation existed. Ideally, a certain morphological phenotype would be associated with a higher potential, while the opposite morphology would associate with low potential. For this purpose, a fluorescence microscopy protocol with subsequent image processing method was utilized. The cell line used was MDA-MB-231, from human mammary adenocarcinoma. Using both simple parameter extraction and cluster analysis, a correlation between potential and morphology was unobservable. This suggests that under normal culture conditions, a cell's morphologically heterogeneous population of mitochondria does not always exhibit the same potential trend. Additionally, a subsequent cell line derived from the parental MDA-MB-231 showing enhanced invasive/metastatic ability was evaluated regarding morphological phenotype, in search of a difference between parental and invasive cell types. A slight difference was found only in the presence of the uncoupling agent CCCP.

Keywords: Mitochondria, potential, morphology, image processing, cluster analysis, heterogeneity

INTRODUCTION

Mitochondria

An eucaryotic cell has different metabolic needs throughout its life. One crucial organelle for the cell metabolism is the mitochondrion. Mitochondria are organelles that are very dynamic in both morphology and function as the needs arise for the cell [1].

Mitochondria are the central organelles responsible for the supply of adenosine triphosphate (ATP) – the cell's source of chemical energy. Additionally, other cellular processes such as the signaling for differentiation and cell death or the control of cell cycle and growth are also largely influenced by mitochondria [2]. They are composed of two different membranes – an outer membrane (OM) and an inner membrane (IM). The protein machinery required for oxidative phosphorylation is organized along the IM (which separates the innermost mitochondrial matrix from the intermembrane space) [3]. Furthermore, mitochondria enclose their own genome (mtDNA), independent from the cell's genome.

Energy production

The most prominent function of the mitochondrion is energy production, through the phosphorylation of adenosine diphosphate (ADP). The series of reactions that comprise a first part of this process is known as the citric acid cycle, tricarboxylic acid (TCA) cycle or Krebs cycle. These reactions take place inside the mitochondrial matrix.

The main function of the TCA cycle is to conserve the chemical energy present in molecules of acetyl-CoA by oxidizing them into carbon dioxide and consequently reducing NAD and FAD (Nicotinamide Adenine Dinucleotide and Flavin Adenine Dinucleotide, respectively – two important redox cofactors) into NADH and $FADH_2$. Concomitantly,

a second part of respiration, oxidative phosphorylation occurs using these two molecules as substrates. This process is performed by a sequence of protein complexes (the electron transport chain – ETC), embedded in the IM [3].

As its name implies, the ETC mediates the flux of electrons. The electron donor molecules for this chain are NADH and $FADH_2$, products of the TCA cycle and glycolysis. The enzyme complexes present in the ETC are then responsible for the passing of electrons through the chain onto a final electron acceptor, O_2 [4].

The aim of this transport of electrons is the creation of an electrochemical gradient through the pumping of protons across the IM by the enzymes that compose the chain. The protons responsible for the gradient are then allowed to return to the mitochondrial matrix through the ATP synthase complex, which is an enzyme that uses the protons' potential energy as they are transported to synthesize ATP from ADP and inorganic phosphate (PO_4^{-3}) [4].

Apoptosis regulation

In addition to being important for their role of energy production, mitochondria are also central players in the regulation of programmed cell death. The basic idea behind this process is that under stress, certain membrane channels are activated and there is a release of apoptogenic proteins into the cytosol, which then start a protease cascade pathway, ending in the degradation of intracellular proteins and nuclear DNA.

Mitochondria play a two-fold role in apoptosis. Cell-internal stimuli such as reactive oxygen species (ROS), are directly mediated by mitochondria. However, studies have shown that mitochondria also play a part in the processing of cell-external stimuli for cell death: the work of *Lassus et al.* [5] demonstrated that external cytokine signalling directly activates caspase 2, in which case the mitochondria functions as an amplifier of the cascade response to the stress [6].

Mitochondrial dynamics

While being generally portrayed as a small bean-shaped organelle, the mitochondrion is actually highly dynamic in nature. In order to meet the metabolic needs of the cell, mitochondria undergo constant fusion and fission, going from small round objects to a fully connected complex network [7]. This allows for a large heterogeneity in mitochondrial morphologies, for instance in different cell types.

The fusion and fission dynamics achieve several purposes, such as mitochondrial distribution and inheritance, mitochondrial remodeling (*e.g.* in tissue development/differentiation) and release of apoptogenic factors for cell death mediation [1].

Mitochondrial dynamics regulatory mechanisms can be divided into four groups: biogenesis, movement, fusion and fission, and mitophagy (Figure 1).

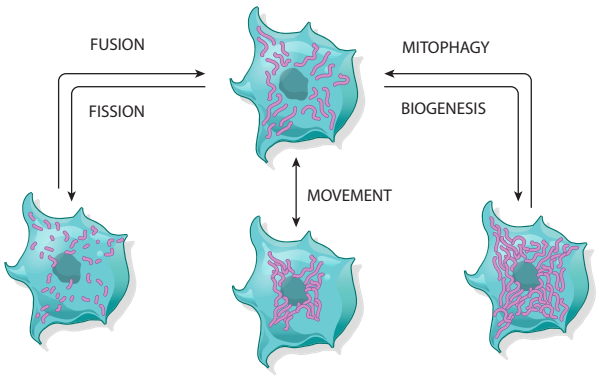

Figure 1: Simple schematic representation of the main mechanisms of mitochondrial dynamics. Adapted from [8].

BACKGROUND

Segmentation methods overview

In order to quantify differences in shape features between two images or sets of images, the raw image data must first be processed. For the shape of mitochondria to be defined, a *binary* image (an image that only has two possible values for each pixel) is usually produced [9].

To obtain such an image, a variety of methods can be used. These methods – that further translate to constructed algorithms – ultimately fall into the following three general steps [10]: pre-processing, detection and measurement.

Pre-processing The processing of obtained raw images is mandatory in almost all cases in order to guarantee the faithful representation of the data that will be analyzed subsequently [10]. The idea behind processing involves the application of a series of filters – each pixel's value is reassigned based on some form of mathematical operation performed on that pixel's defined neighborhood. Convolution filtering can be easily visualized by taking a convolution kernel (the actual filter that is used to calculate the new value for each pixel) and overlaying it on the original image.

Detection The task of detection is usually to automate what could be done manually by hand-drawing regions-of-interest (ROIs) on the image under analysis. The simple motivation behind this is that it has the advantage (if correctly built) of giving reproducible and less biased results. In addition, it is obviously much faster, rendering it com-

pulsory when doing analysis of large populations of objects. Performing the detection of objects is mostly termed image *segmentation*.

In the large majority of the cases in image processing, this segmentation step of the process proves to be the most difficult. The critical challenge is usually to find either a threshold or a thresholding method in order to accurately detect the objects of interest.

One of the most commonly used techniques for finding a threshold value automatically is Otsu's method [11]. What this method does, is computing the threshold that minimizes the intra-class variance (variance withing each class, $\sigma_w^2(t)$):

$$\sigma_w^2(t) = \omega_1(t)\sigma_1^2(t) + \omega_2(t)\sigma_2^2(t) \tag{1}$$

Where $\omega_i(t)$ are the weigths of the classes, σ_i^2 are the class variances and t is the chosen threshold value.

Measurement When the finalized binary or labeled image is obtained, the last step to perform is the analysis or measurement of desired features. In this work, the main analyzed features of interest pertaining to detected mitochondria were area, aspect ratio and roundness. Below we provide working definitions:

Area (A) The number of connected pixels within an object.

Aspect Ratio ($\mathcal{AR}$) The aspect ratio is usually taken as the ratio between the major and minor axis lengths of the ellipse that shares the same second central moment (i.e. variance) with the region in analysis [9]. This classical definition presents a crucial problem in the case of mitochondria analysis: since mitochondria are generally tubular shaped objects of highly variable length and deformable, they may appear as concave objects in 2D images, which will give rise to erroneously calculated values of aspect ratio. Consequently, the aspect ratio was defined to be:

$$\mathcal{AR} = \frac{\pi}{4}\frac{L}{l} = \frac{\pi}{4}\frac{L^2}{A} \tag{2}$$

Here, L is the skeleton length and l is the average width of the object (minor axis length, in the case of an ellipse). It is trivially proven that for a circle, this ratio equals 1.

Determining the skeleton length was done by morphological *thinning*, which iteratively removes pixels from the outermost part of an object (for the obtainment of the skeleton, the operation is run until the there are no more pixels to remove): in MATLAB, `bwmorph(BW,'thin',Inf)`, where BW is the binary image.

Roundness (R) Roundness is frequently interchanged with the terms sphericity, circularity, form factor and compactness, for example. In this work, the importance of roundness is to be able to assess how similar the mitochondrial shape is to a circle [12, 13, 14]. There are a few similar ways of approaching this objective, but the following definition reaches this exact purpose:

$$R = \frac{4\pi A}{P^2} \tag{3}$$

However, due to the technical way that the value for the Perimeter is computed in the Image Processing Toolbox of MATLAB, this formula overestimates the roundness for every object. In short, the perimeter is estimated using pixel centers as opposed to pixel boundaries. A simple correction can address this problem, assuming circular objects, adding π to the perimeter effectively amends the roundness value [15].

The rectified formula is then:

$$R = \frac{4\pi A}{(P+\pi)^2} \tag{4}$$

MATERIALS AND METHODS

Cell culture

Human mammary adenocarcinoma cells derived from the metastatic site (MDA-MB-231) were cultured in DMEM medium (Gibco, Life Technologies, USA) with 10% Fetal Bovine Serum (FBS) (HyClone, Thermo Fisher Scientific, USA) and 100 U of penicillin/100 g of streptomycin (Sigma-Aldrich, USA). The cell culture was performed in a 37° C, humidified, 5% CO_2 environment. Cells were passaged when reaching 70% confluency. Cell passaging consisted in washing the culture with Phosphate-Buffered Saline (PBS) (Gibco, Life Technologies, USA), detaching the cells with 0.25% Trypsin in HBSS (Mediatech, USA) for 5-10 min, adding fresh medium to neutralize trypsin activity and seeding the desired fraction of cells onto a new culture dish.

Mitochondrial stain

MTr (MitoTracker Red CMXRos, M-7512, Thermo Fisher Scientific, USA) and the anti-TOMM20 (FL-145, Santa Cruz Biotechnology) antibody were chosen for the fixable stain method. One advantage of MTr is its ability to be fixed after staining, allowing for the usage of other fixable stains in tandem. The protocol was extended to include not only these two fluorescent signals, but also Hoechst 33342 (H3570, Thermo Fisher Scientific, USA) and Phalloidin 647 (A22287, Thermo Fisher Scientific, USA) which stain for the nuclei and F-actin (cytoskeleton) respectively.

For the staining of cell cultures, the staining media is always pre-incubated for 1 h in the same CO_2 incubator used for culture. For the CCCP-treated (carbonyl cyanide m-chlorophenyl hydrazone, C2759, Sigma-Aldrich, USA) conditions, a stock solution is first prepared by dissolving the CCCP in DMSO (Dimethyl sulfoxide) to a 100 mM concentration which is then used to prepare the final drug solution by dilution in culture medium to a final concentration of 50 µM. The MTr stock solution was prepared in DMSO to a 500 µM concentration. CCCP 50 µM solution was added to the pertinent cell culture dishes 20 min before staining with MTr. Control dishes were then stained with 200 nM MTr solution (diluted in staining medium from stock solution) and CCCP dishes are stained with a staining solution containing both 200 nM MTr and 50 µM CCCP. The cells were incubated with the staining solutions for 45 min in the CO_2 incubator (protected from light). One wash cycle is then performed with pre-incubated medium, before adding a 4% PFA (Paraformaldehyde, 28906, Thermo Fisher Scientific, USA) (in PBS) fixing solution for 20 minutes at room temperature. After 1 wash cycle with PBS, a 0.1% Triton X-100 (X100, Sigma-Aldrich, USA) solution (in PBS), is then used to permeabilize the cells. Another PBS wash-cycle is performed and a 1% BSA (Bovine serum albumin) blocking solution (in PBS) is used for 2 h at room temperature. The anti-TOMM20 primary antibody (FL-145, Santa Cruz Biotechnology) is then used at a 1:50 dilution ratio in 1% BSA for 16 h at 4°C. Lastly, after 3 wash cycles with PBS, Phalloidin 647, Hoechst 33342 and goat anti-Rabbit IgG secondary antibody Alexa Fluor 488 conjugate (A-11008, Thermo Fisher Scientific, USA) are added at 1:50, 1:40 and 1:200 dilutions respectively, in 1% BSA, for 1 h at room temperature. Fix-and-stained samples are then kept in PBS at 4°C until imaging. The imaging of the samples was conducted within 1 week of staining.

For live-cell imaging, the TMRE (Tetramethylrhodamine Ethyl Ester, T-669, Molecular Probes, USA) and MTg (MitoTracker Green FM 9074, Cell Signaling Technology) combination was chosen. Both dyes were stored in DMSO at 4.85 mM and 500 µM concentrations respectively, at 4°C. The final concentrations were prepared in cell culture medium and were 100 nM MTg and 25 nM TMRE. The staining solutions were added consecutively, MTg first for 45 min and then TMRE for 15 min before the start of imaging, always in the incubator at 37°C. Imaging was performed with a live-cell unit to maintain cell-culture conditions during the process. Cells were maintained in the TMRE staining solution throughout the imaging, to allow for the maintenance of the equilibrium of the dye between mitochondria, cytosol and external medium.

Cell imaging

Cultures for imaging were performed on 35mm glass-bottom culture dishes (Stemcell Technologies). Imaging was executed on a Nikon A1R$^+$ confocal fluorescence microscope, with a 100× objective (CFI Plan Fluor DLL 100X Oil, Nikon) and Nikon Ti ZDrive and XYDrive. Multichannel imaging was done sequentially. No FRET was found between MTg and TMRE at the concentrations used. The channel series was set to guarantee no bleed-through of fluorescence from unwanted fluorophores.

RESULTS

From all the available literature that involves mitochondrial morphology in conjunction with mitochondrial potential, a conclusion can be commonly drawn: mitochondrial morphology and mitochondrial potential are correlated with each other. Despite this fact being thoroughly established, it is based on observations of mitochondrial properties (morphology and potential) after some kind of external influence – drugs, growth factors, media composition, substrate stiffness, etc... [16]

The present study also intended to find if there was a significant difference in mitochondrial morphology and potential between two different cell lines. The cell lines were from MDA-MB-231 cells, where cell line sc0 was the unaltered cell line, and sc308 was derived from the first through single-cell cloning. The two cell lines were proven to be phenotypically different, varying in metastatic capacity, for instance.

In addition to the previous objective, this work aims to conclude if the correlation between mitochondrial potential and morphology is observable in the absence of external influence – i.e. in the same cell population, is there a significant tendency between different morphological features and mitochondrial potential?

Adaptive Local Normalization based segmentation

Concept Out of a number of different methods, *Adaptive Local Normalization* (ALN) enhancement for segmentation was a promising candidate for the type of data this analysis entailed. It was developed by *Peng et al.* [17] as an image enhancement method capable of correcting variant background intensity abnormalities.

Fluorescence microscopy produces images with inhomogeneous background intensity, as a consequence of out-of-focus objects and non-optimal dye staining of the samples, originating a spill-out of the fluorescence into the background. Making use

of confocal microscopy helps to greatly reduce the issue, but may commonly not be sufficient for some analyses (i.e. very small organelles, dense cell bodies, small cytosolic volume). In these cases, ALN enhancement may be a suitable tool to address the obstacle.

The proposed method [17] not only makes use of local thresholding, but goes one step further by adaptively changing the size of the pixel neighborhood used. ALN uses the statistical properties of each local neighborhood in order to correctly assess the adequate neighborhood size. The aim of letting the filtering window dynamically change its size is to guarantee that regions for pixels within an object of interest contain some area of background and regions for background pixels contain portions of objects. Simply, every region should be sufficiently large to contain features from nearby objects. This way, each pixel neighborhood will contain enough information for a correct classification into object or background [17].

Peng et al. [17] proposed using the statistical pixel region variance of intensity values as the criterion to determine the suitable region size. Mathematically, this translates for each pixel (x, y) to:

$$r(x,y) = \min_r \{r > 0 : \sigma(R_r(x,y)) \geq T_\sigma\} \tag{5}$$

Where $r(x, y)$ is the radius of the disk-shaped region $R_r(x, y)$ at position/pixel (x, y), σ is the standard deviation and T_σ is the standard deviation threshold defined for the algorithm (i.e. an input variable). In this particular work, it was chosen to set the threshold in relation to the standard deviation of the whole image, $\sigma(I) = \sigma_I$,

$$T_\sigma = k_\sigma \cdot \sigma_I \tag{6}$$

where k_σ is simply a coefficient of the global standard deviation. A reasonable range for k_σ is from 0.2 to 0.8 [18]. An assumption is then made that if a region has a standard deviation larger than T_σ, it contains enough structures of interest and background to make the distinction between the two.

The enhanced image is then obtained through a normalization operation over the original image and the mean- and standard deviation- filtered images with respect to the region sizes found previously:

$$I_\mu(x,y) = \langle R_r(x,y) \rangle \tag{7a}$$

$$I_\sigma(x,y) = \sigma\left(R_r(x,y)\right) \tag{7b}$$

$$I_{ALN}(x,y) = \frac{I(x,y) - I_\mu(x,y)}{I_\sigma(x,y)} \tag{7c}$$

Where I_μ is the mean-filtered image (i.e. average-filtered), I_σ is the standard-deviation filtered image and I_{ALN} is the image enhanced through ALN. After I_{ALN} is obtained, any thresholding method may be applied to obtain the binary image with the segmented objects.

If no computational limitations existed, the algorithm would iterate values of r until infinity. However, in reality, it does not make sense to do such calculations. A maximum radius, r_{max} is thus set to account for this event. This limitation gives origin to a new problem that is relatively easy to resolve: large low variance regions will be highlighted. Simply setting a minimum standard deviation, $\sigma_{min} = T_\sigma$, for regions that would exceed the maximum radius covers this matter. Rectifying the respective equations, we have:

$$r(x,y) = \min\left\{r_{max}, \min_r \{r > 0 : \sigma(R_r(x,y)) \geq T_\sigma\}\right\} \tag{8}$$

$$I_\sigma(x,y) = \max\left\{T_\sigma, \sigma\left(R_r(x,y)\right)\right\} \tag{9}$$

Implementation As common practice in the image processing area, before the actual segmentation is performed, a number of pre-processing steps may be set-up. In the present case, it was important to remove some noise in the data. Otherwise, the noise could have a nefarious impact in the statistical properties of the local regions found to be adequate. There are a large variety of noise-removal approaches. For this particular application, a Fourier low-pass filter was found to be effective.

Concerning the actual implementation of the ALN enhancement, the first step to be executed is to create the data needed for the enhancement. For simplicity purposes, it was chosen to create this data for the whole range of radii, r, and only then choosing the data to use. As such, the code is executed as described in Algorithm 1.

Expressly, three variables are initiated to begin with. R_{map} is a 2-Dimensional "map" that will be used to hold the radius values that meet the ALN conditions at each pixel location, $S_\sigma(x, y, r)$ and $S_\mu(x, y, r)$ are, similarly, 3-Dimensional "maps" that will hold the standard deviation and mean values for each region size (each layer of the 3D array contains the information for one radius). The for-loop is used to calculate these variables. The 3D arrays are built layer by layer, while R_{map} is updated in each loop in order to minimum value of r found to meet the condition $S_\sigma(x, y, r) > T_\sigma$ until that point. In the positions where the condition was not met, the value is kept at r_{max}. Finally the images needed for the ALN enhancement, I_σ and I_μ, are created from the gathering the appropriate values of σ and μ using the r values in R_{map} as an index for the layers to access in the 3D arrays, for

Algorithm 1 Adaptive Local Normalization implementation

1: Initiate R_{map} as a 2-Dimensional holding the maximum value r_{max} in every location
2: Initiate S_σ, S_μ as 3-Dimensional arrays, width and height equal to I, depth being the number of steps of r
3: **for** $r = r_{min}$ to r_{max} **do**
4: nhood $\leftarrow$ disk of radius r
5: $S_\sigma(x, y, r) \leftarrow \text{STDFILTER}(I, \text{nhood})$
6: $S_\mu(x, y, r) \leftarrow \text{MEANFILTER}(I, \text{nhood})$
7: Initiate R_{temp} as a 2-Dimensional
8: In R_{temp}, assign r to pixels where $S_\sigma(x, y, r) > T_\sigma$
9: In R_{temp}, assign r_{max} to pixels where $S_\sigma(x, y, r) < T_\sigma$
10: Update $R_{map} \leftarrow min\{R_{map}, R_{temp}\}$
11: **end for**
12: Assign to I_σ and I_μ the correct values of σ and μ fetched from the page of index r indicated in R_{map} of S_σ and S_μ
13: Assign $I_{ALN} = \dfrac{I - I_\mu}{I_\sigma}$

each location.

After the enhancement has been executed, a fitting segmentation method may be applied. Otsu's method was chosen, in this case, also recommended by *Peng et al.* [17]. Some posterior processing was then needed to discard some objects that were picked up even though they are too dim or too small to be relevant. Objects are first discarded if they are touching the image's borders, since their properties would be wrongly reported. Secondly, objects that are under a certain pixel size threshold (their area) are also ignored. Lastly, objects whose intensity falls below a certain threshold should also be neglected.

The process was thus defined as follows:

Algorithm 2 Post processing

1: Extract the mean-intensity value for every object in I_{BW}
2: Define an input threshold value, k_{int}
3: Calculate the median value for the entire object population, z_{med}
4: Delete every object whose mean-intensity is lower than $k_{int} \cdot z_{med}$

By being defined this way, the post processing takes into account the mean-intensity of each object, guaranteeing that no information is being lost because sporadic pixels inside an object are very dim.

In Figure 2 the process described so far can be seen as applied to an actual microscopy image sample. In the same figure, all images except R_{map} are represented in greyscale, with the brightest value being white and darkest being black. I^*_{BW} corresponds to the Otsu's thresholding of I_{ALN} before post-processing applied. I_{BW} is the final processed image.

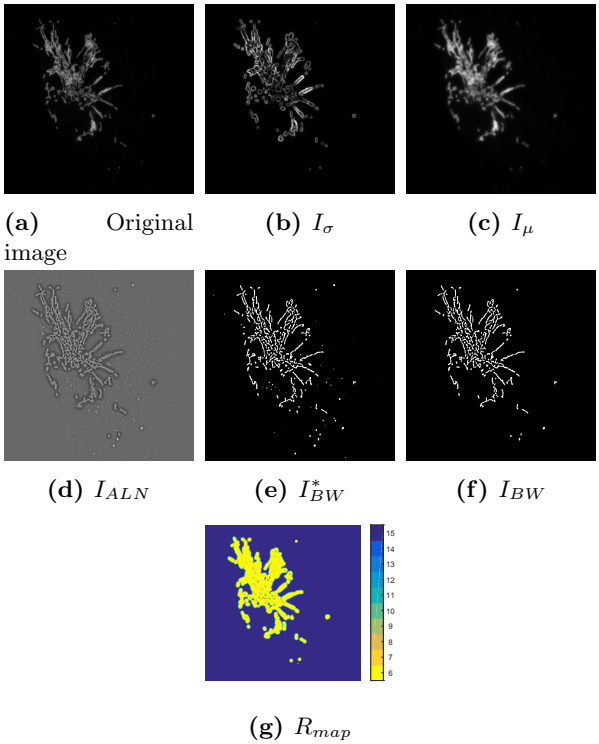

(a) Original image **(b)** I_σ **(c)** I_μ

(d) I_{ALN} **(e)** I^*_{BW} **(f)** I_{BW}

(g) R_{map}

Figure 2: The application of Adaptive Local Normalization segmentation to a fluorescence image (a). (b) – standard-deviation filtered image, I_σ. (c) – mean-filtered image, I_μ. (d) – ALN-enhanced image, I_{ALN}. (e) – result of thresholding I_{ALN} using Otsu's method, I^*_{BW}. (f) – final result, after post-processing, I_{BW}. (g) – the R_{map} radius value map originated from the conditions of the ALN method.

Classification Dimensionality reduction usually aids interpretation or comprehension of a system that may be convoluted but have some redundancy in its descriptors. Cluster analysis is most useful on clearly sub-divided systems, but is also helpful to gain an intuitive view of data that is not only purely mathematical, but contains some real-world implications (biological in this case).

K-means clustering is one method of achieving such a task. For data that is naturally branched into a set number of groups, choosing the input number of clusters is trivial. However, this is only routinely the case for data extracted from distinctly different sources.

After applying PCA to the entire group of mor-

phological parameters extracted from control cells in this study (data not shown), no clear definition between different groups is observable. This reflects on the original data such that at first glance, there should be no clear number of clusters in which to divide the analysis. The breakdown of the data in different fragments still provides an intuitive way of looking into the system. Thus clustering will be used with 3 artificial k-means clusters ordered according to their average properties into: Fragmented, Intermediate, Elongated. The 3 clusters will be colored Red, Green and Blue in the respective order: Fragmented, Intermediate, Elongated.

System validation

In the field, in order to demonstrate that the method built for reporting mitochondrial potential/morphology is in fact sensible to disruptions, a range of drugs can be used. One of the most common ones is carbonyl cyanide m-chlorophenyl hydrazone (CCCP). This drug is an ionophore which allows for the transport of protons through lipid bilayers. The biological result of adding the ionophore to a cell population is the direct counteraction of the proton gradient. As a consequence, the mitochondrial potential is depleted. This mitochondrial uncoupling causes the rapid fragmentation of the mitochondria into small punctate bodies [19].

For the simultaneous visualization/measurement of both mitochondrial potential and morphology on a fluorescent microscope, two mitochondrial dyes are needed. For the primary objective of discovering differences between the two cell lines, Mitotracker Red was chosen for reporting potential, and a primary anti-TOMM20 antibody for morphology, later stained with a labeled secondary antibody. The reasoning behind the two dyes is twofold. In the absence of mitochondrial potential, the potential-independent dye is needed in order to still be able to obtain mitochondrial shape. Additionally, since this method is purely optical, the potential-independent also serves as a way of normalizing the potential signal of each mitochondrion. A simple example of why the latter is important is out-of-focus light: since potential will be measured from the fluorescence intensity, lower intensities due to slightly out-of-focus light have to be normalized. Otherwise, an underestimated reading of intensity/potential would arise from objects that are not perfectly aligned to the focal plane, which is unavoidable in practice. Figure 3 showcases the effect of CCCP in cells from the sc0 cell line visualized using the described dyes. The almost complete absence of MTr fluorescence signal in the CCCP-treated cells is notable – being depolarized, the mitochondria did not incorporate the dye. Also, the fragmented phenotype of the mitochondria in the same condition is also in accordance with current knowledge [19].

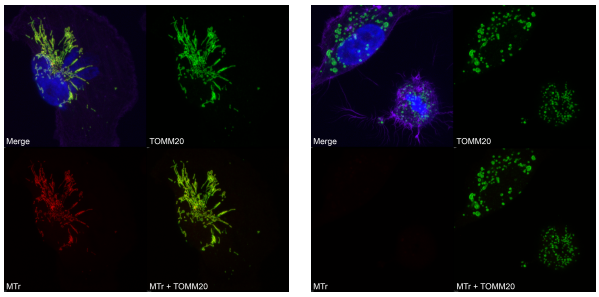

(a) Control **(b)** 50 µM CCCP, 20 min

Figure 3: Fluorescence image of the effects of the uncoupling drug CCCP on sc0 cells. The *Merge* image is the joint visualization of the MTr (red) and TOMM20 (green) as well as F-actin (purple) and nucleus (blue). Note the extremely low MTr fluorescence and the fragmented globular shape of mitochondria in the CCCP-treated cells.

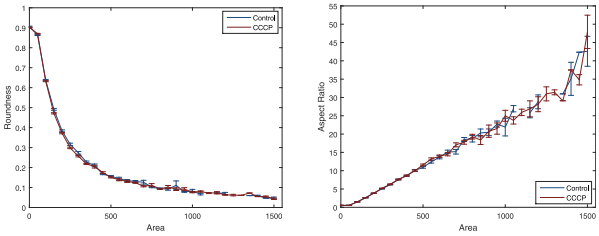

(a) Control **(b)** 50 µM CCCP, 20 min

Figure 4: Correlations between the main morphological parameters extracted from control and CCCP-treated cells. The conditions have overlapping curves, despite the difference in relative number of small/large mitochondria between the two. The tendencies follow the expected trend for tubular objects – roundness lowers as the tubule grows larger and aspect ratio increases. Each data point in the curves represents the calculated average of all values in the corresponding bin (bin size = 50). Error bars represent standard error.

Before proceeding with the results, it is important to guarantee the system is behaving in a consistent way and correctly reports the variables of interest. To this degree, the tendency in the parameters from the populations of mitochondria of both cell types were examined. The results of plotting the parameters of all the single mitochondria can be seen in Figure 4. The correlation between the parameters is followed as expected for tubular-like objects such as mitochondria – as the area of the object increases, the roundness decreases (typically round mitochondria are also fragmented/punctate) and the aspect ratio increases (the width is generally maintained as

the length of the mitochondria increases). Furthermore, the correlation is preserved for control and CCCP (even if the relative quantity of long/non-round mitochondria is much lower).

Another way of evaluating the data is to consider the clusters/classes created instead of the single variables. Again, the logical correlations are observable (Figure 5). Interestingly, by plotting the normalized signal of $\frac{\text{Mitotracker Red}}{\text{TOMM20}}$, the absence of correlation between Mitochondrial potential and the morphological clusters is already suggested, although this matter will be further discussed onward.

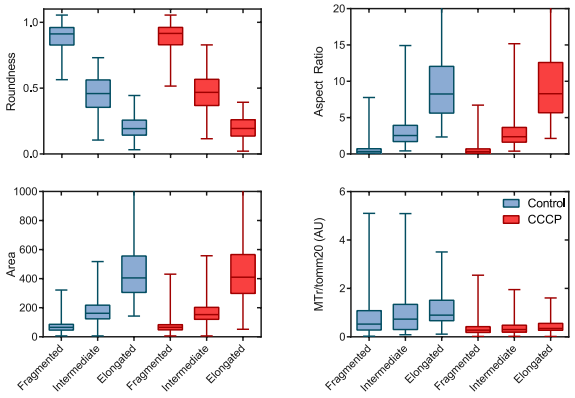

Figure 5: Correlations between the main morphological parameters along with the normalized signal of potential and the 3 generated morphological clusters. The boxes denote the data from 25th to 75th percentiles. Error bars denote the minimum and maximum values in each cluster.

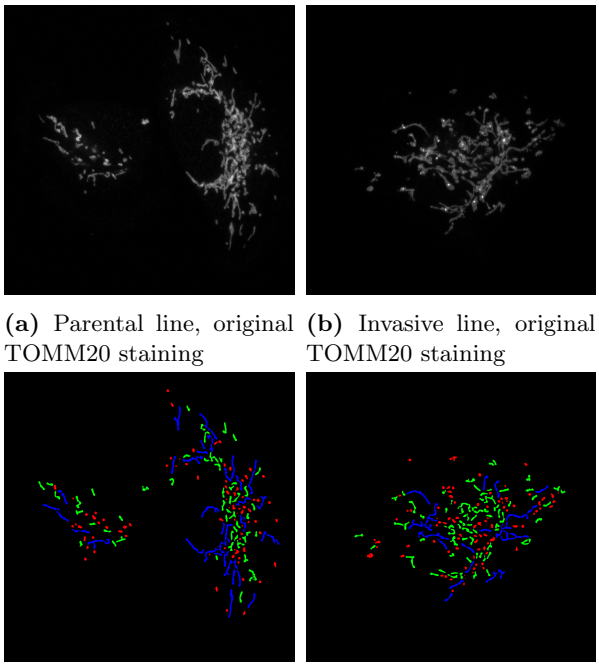

(a) Parental line, original TOMM20 staining

(b) Invasive line, original TOMM20 staining

(c) Parental line, segmentation and classification results

(d) Invasive line, segmentation and classification results

Figure 6: Representative images of the TOMM20 mitochondrial staining of cells from parental and invasive cell lines. The bottom row shows the segmentation and classification result of the top images. The colors red, green and blue represent fragmented, intermediate and elongated morphological clusters, respectively.

Difference between cell lines

For the purpose of finding a possible difference in mitochondrial morphology and potential between the two cell lines, they were cultured in identical conditions, in parallel. After staining the cultures appropriately with Mitotracker Red and the secondary antibody (as well as Hoechst 33342 for nuclei and labeled Phalloidin for cytoskeleton), the samples were imaged. In addition to the normal control samples, another condition was studied by subjecting the cells to 50 µM of CCCP for 20 min prior to staining.

Figure 6 provides two representative examples of the images obtained of the mitochondria in the two cell lines (sc0 - Parental, sc308 - Invasive). While the images alone don't show a striking difference through simple visual analysis, the extraction of morphological descriptors could give more significant insight. Thus, after segmentation and classification of the mitochondria populations in the images, the fractions of fragmented, intermediate and elongated mitochondria could be assessed between the various conditions (Figure 7).

The results shown in Figure 7 suggest that there is a difference in response to CCCP between the Parental and Invasive cell types. The morphological phenotype between both control conditions show no significant difference, implying that the increased metastatic ability may originate elsewhere. Studying different drugs using the same method may provide interesting new results on the response of the Invasive cell type to treatment.

Mitochondrial morphology and potential correlation

The various existing dyes available for mitochondrial inevitably have different characteristics and are more or less appropriate to different applications according to them. While Mitotracker Red is pertinent for use to study overall mitochondrial potential for populations under one unchanged condition, it falls short if one intends to interfere with the system or measure dynamic changes in the potential. The Mitotracker Red molecule possesses a clorometyl thiol-reactive moiety, which will react with proteins [20].

A different dye is required to monitor potential dynamically in mitochondria. One possible solu-

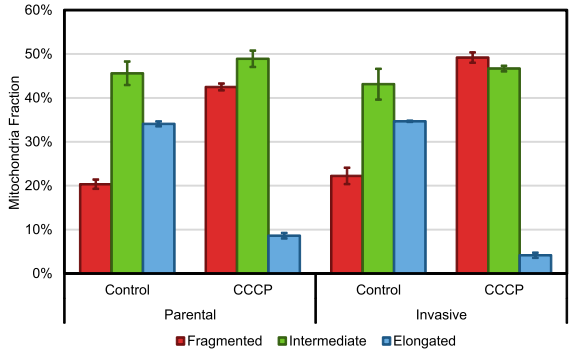

Figure 7: Fractions of mitochondria in the fragmented, intermediate and elongated morphological clusters for the parental and invasive cell lines under control and CCCP conditions. The CCCP condition was characterized by treatment with 50 µM CCCP for 20 min in culture. There is no significant difference between the two cell lines in control condition. There is a ~8% difference in fragmented mitochondria between the two CCCP cases, suggesting a different morphological response to the drug.

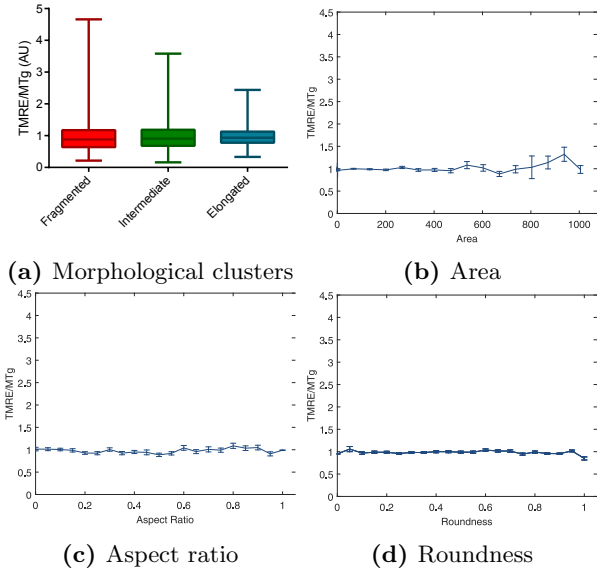

(a) Morphological clusters **(b)** Area

(c) Aspect ratio **(d)** Roundness

Figure 8: Results of morphological analysis on the live-cell mitochondrial potential stain. Both the cluster analysis (a) and the single morphological parameters (b – d) show no observable correlation with normalized mitochondrial potential. Each data point in the curves on (b – d) represents the calculated average of all values in the corresponding bin (bin size for (b) = 67, bin size for (c,d) = 0.05). Error bars represent standard error.

tion is TMRE (Tetramethylrhodamine ethyl ester), a lipophilic cationic dye that exhibits very little binding to the mitochondrial membranes, and accumulates in the mitochondria according to the Nernst equation [20]. A simultaneous potential-independent dye is still needed. Mitotracker Green comes as a carbocyanine-based dye that is widely reported to be independent on mitochondrial membrane potential [21]. It is also fully usable in live-cell experiments, as long as the concentration is kept at low values to discard cytotoxicity (as is the case for most dyes).

Making sure the previous aspects are covered, the cells loaded with Mitotracker Green and TMRE may be subjected to the same analysis as before. By performing morphological clustering on the segmented mitochondria and looking into the normalized intensity signals for mitochondrial potential ($\frac{\text{TMRE}}{\text{MTg}}$), the correlation with morphology, if any, should be readily observable.

The results of this assay are summarized in Figure 8, where the potential signal is evaluated against both the single morphological parameters used and the morphological clusters from k-means clustering.

From the results from all the variables and the morphological clusters in Figure 8, no correlation is observable between morphology and potential. Despite the existence of some variance in the potential for each morphological cluster, the mean value is not significantly different (the positive and negative "errorbars" in the cluster plot represent maximum and minimum values for each cluster). The same is true for single variables, where there is high variance, but the very large majority of the mitochondria follow a zero-slope tendency (the errorbars presented for single variables represent standard error).

CONCLUSIONS

Through the usage of Adaptive Local Normalization, image quality complications could be overcome, allowing for the segmentation of single mitochondria from high-magnification fluorescence microscopy image. In turn, this segmentation further allowed the extraction of both single-mitochondria morphological parameters and mean fluorophore intensity (dependent and independent of potential).

From the observation of the results of the mitochondrial morphology clustering, a difference between the Parental, sc0, and Invasive, sc308, cell lines was not found in control culture conditions. By subjecting the cell culture to the uncoupling drug CCCP, a relative morphology difference was found, suggesting that the cell types may have an inherently different drug response, with the Invasive line exhibiting a higher percentage of Fragmented mitochondria in presence of the drug. In order to solidify and gain further insight into this finding an array of mitochondria-targeted drugs can be used.

Furthermore, when exploring the possible correlation between mitochondrial morphology and potential, based on potential-dependent probes, we observed that the normalized intensity signal for potential did not correlate with mitochondrial area, aspect ratio or roundness. Consistently, the clusters generated from the multivariate morphological data also did not correlate with mitochondrial potential. This suggests that the morphologically heterogeneous population of mitochondria within a cell does not always exhibit the same trend.

References

[1] Benedikt Westermann. Bioenergetic role of mitochondrial fusion and fission. *Biochimica et Biophysica Acta (BBA)-Bioenergetics*, 1817(10):1833–1838, 2012.

[2] Heidi M McBride, Margaret Neuspiel, and Sylwia Wasiak. Mitochondria: more than just a powerhouse. *Current Biology*, 16(14):R551–R560, 2006.

[3] Stefan Krauss. Mitochondria: Structure and role in respiration. *eLS*, 2001.

[4] D Voet, J Voet, and C Pratt. Fundamentals of biochemistry. *Hoboken: Wiley*, 2006.

[5] Patrice Lassus, Ximena Opitz-Araya, and Yuri Lazebnik. Requirement for caspase-2 in stress-induced apoptosis before mitochondrial permeabilization. *Science*, 297(5585):1352–1354, 2002.

[6] Bernd Mayer and Rainer Oberbauer. Mitochondrial regulation of apoptosis. *Physiology*, 18(3):89–94, 2003.

[7] Richard J Youle and Mariusz Karbowski. Mitochondrial fission in apoptosis. *Nature reviews Molecular cell biology*, 6(8):657–663, 2005.

[8] Scott B Vafai and Vamsi K Mootha. Mitochondrial disorders as windows into an ancient organelle. *Nature*, 491(7424):374–383, 2012.

[9] Rafael C Gonzalez and Richard E Woods. Digital image processing, 2002.

[10] Peter Bankhead. Analyzing fluorescence microscopy images with imagej. 2014.

[11] Nobuyuki Otsu. A threshold selection method from gray-level histograms. *Automatica*, 11(285-296): 23–27, 1975.

[12] John J Friel et al. *Practical guide to image analysis*. ASM international, 2000.

[13] Twan Maintz. Digital and medical image processing. *Universiteit Utrecht*, 2005.

[14] Wilhelm Burger and Mark J Burge. *Digital image processing: an algorithmic introduction using Java*. Springer Science & Business Media, 2009.

[15] Chris Luengo. Measuring boundary length, July 2015. URL `http://www.cb.uu.se/~cris/blog/index.php/archives/310`.

[16] Kurt J De Vos, Victoria J Allan, Andrew J Grierson, and Michael P Sheetz. Mitochondrial function and actin regulate dynamin-related protein 1-dependent mitochondrial fission. *Current Biology*, 15(7):678–683, 2005.

[17] Jyh-Ying Peng, Chung-Chih Lin, and Chun-Nan Hsu. Adaptive image enhancement for fluorescence microscopy. In *Technologies and Applications of Artificial Intelligence (TAAI), 2010 International Conference on*, pages 9–16. IEEE, 2010.

[18] Qiang Wu, Fatima Merchant, and Kenneth Castleman. *Microscope image processing*. Academic press, 2010.

[19] Naotada Ishihara, Akihiro Jofuku, Yuka Eura, and Katsuyoshi Mihara. Regulation of mitochondrial morphology by membrane potential, and drp1-dependent division and fzo1-dependent fusion reaction in mammalian cells. *Biochemical and biophysical research communications*, 301(4):891–898, 2003.

[20] Tetsuhiro Minamikawa, Absorn Sriratana, David A Williams, David N Bowser, John S Hill, and Phillip Nagley. Chloromethyl-x-rosamine (mitotracker red) photosensitises mitochondria and induces apoptosis in intact human cells. *Journal of Cell Science*, 112(14):2419–2430, 1999.

[21] W Pendergrass, N Wolf, and M Poot. Efficacy of mitotracker green and cmxrosamine to measure changes in mitochondrial membrane potentials in living cells and tissues. *Cytometry Part A*, 61(2): 162–169, 2004.